Stress measurements in crystalline rock: Comparison of overcoring, hydraulic fracturing and induced seismicity results

Conference Paper · June 2017

CITATIONS
15

READS
585

7 authors, including:

Hannes Krietsch
RWTH Aachen University
58 PUBLICATIONS **664** CITATIONS
SEE PROFILE

Valentin Gischig
ETH Zurich
120 PUBLICATIONS **2,223** CITATIONS
SEE PROFILE

Mohammadreza Jalali
RWTH Aachen University
117 PUBLICATIONS **800** CITATIONS
SEE PROFILE

Keith Evans
ETH Zurich
108 PUBLICATIONS **4,101** CITATIONS
SEE PROFILE

ARMA 17-XXXX

Stress measurements in crystalline rock: Comparison of overcoring, hydraulic fracturing and induced seismicity results

Krietsch, H., Gischig, V., Jalali M.R., and Amann, F.
Geological Institute, ETH Zurich, Switzerland
Evans, K.F. and Doetsch, J.
Geophysical Institute ETH, Zurich, Switzerland
Valley, B.
Center for Hydrogeology and Geothermics, University of Neuchâtel, Switzerland

This paper was prepared for presentation at the 51st US Rock Mechanics / Geomechanics Symposium held in San Francisco, California, USA, 25-28 June 2017. This paper was selected for presentation at the symposium by an ARMA Technical Program Committee based on a technical and critical review of the paper by a minimum of two technical reviewers. The material, as presented, does not necessarily reflect any position of ARMA, its officers, or members. Electronic reproduction, distribution, or storage of any part of this paper for commercial purposes without the written consent of ARMA is prohibited. Permission to reproduce in print is restricted to an abstract of not more than 200 words; illustrations may not be copied. The abstract must contain conspicuous acknowledgement of where and by whom the paper was presented.

ABSTRACT: In preparation of a decameter-scale fault stimulation experiment at the Grimsel Test Site, Switzerland, a comprehensive rock stress characterization survey was conducted. The survey combines overcoring of CSIRO-HI and USBM probes with hydrofracture measurements with concomitant monitoring of the induced microseismicity. Impression packer surveys were run following the hydrofracture tests to determine the orientation of the induced fracture at the wellbore. The orientation of the fracture away from the wellbore was determined from the pattern of the microseismicity. The use of a transverse isotropic model for inverting the strains measured during overcoring was essential to obtain stress solutions that were consistent with the hydrofracture and microseismicity results. The indicate that the minimum principal stress, σ_3, is sub-horizontal and oriented north-south. The maximum principal stress, σ_1, dips at 30-40° to the east and has a magnitude of 13-17 MPa. The magnitude of σ_2, is similar to σ_3, and lies in the range 8-10 MPa.

1. INTRODUCTION

To accelerate the development of Enhanced Geothermal System (EGS) technology, the In-situ Stimulation and Circulation (ISC) experiment is being conducted at the Grimsel Test Site (GTS), Switzerland to investigate fundamental processes activated by injections into pre-existing faults and shear zones. This decameter scale experiment aims to address open questions concerning induced seismicity, permeability enhancement, and hydro-mechanical fault response during deep EGS reservoir stimulation operations. Further information can be found in Amann et al. (2017).

Knowledge of the in-situ stress situation within the rock mass is crucial to the design of the experiment and the eventual interpretation of the data, since stress dictates whether slip will occur on pre-existing discontinuities in response to the elevated pressure of the injections, and also controls the magnitude and direction. Thus, a stress measurement campaign that combined stress relief and hydraulic methods was conducted in three differently oriented boreholes (Figure 1). Borehole SBH-1 was drilled with a slight inclination to vertical of 15° towards N260°E, the best-estimate for the direction of σ_3 suggested by Pahl et al., (1989) and Konietzky (1995). The SBH-3 borehole was drilled sub-horizontally towards the "best-estimate" direction of σ_2 with the goal of obtaining a direct measure of the sub-vertical stress from the hydrofracture stress tests. SBH-1 and SBH-3 were drilled into nearly undisturbed rock to observe the stress conditions in the 'far-field' of the shear zone. The SBH-4 borehole was sub-horizontal and drilled orthogonal to SBH-3 so as to penetrate one of the shear zones that were the target for the stimulations with the objective of identifying potential stress changes towards the fault.

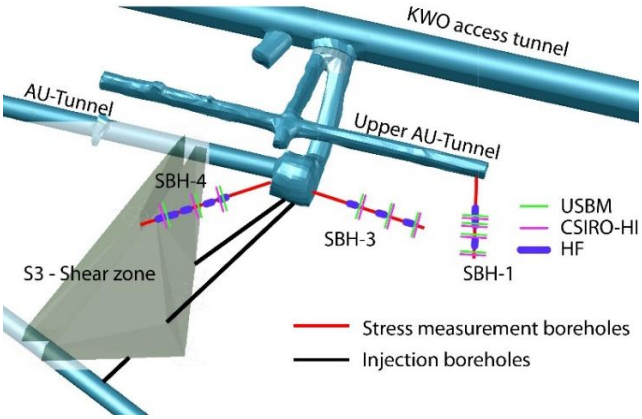

Figure 1 - Locations of stress measurements and boreholes. The lines indicate the stress measurement boreholes (red), injection boreholes (black), USBM-probe (green), CSIRO-HI-probe (purple), and HF-locations (blue). Additionally, the target shear zone (S3) is indicated.

2. GEOLOGICAL SITE DESCRIPTION

Within the GTS, the ISC experiment is located at the lithological boundary between the Central Aare Granite and the Grimsel Granodiorite, both of which are moderately metamorphosed igneous rocks. The ISC test volume is located within a relatively undisturbed foliated rock mass (i.e. very few small-scale fractures), which is crosscut by five major sub-vertical ductile shear zones. Three of these shear zones follow a NE-SW strike (i.e. so-called S1 shear zones) and two an E-W strike (i.e. so-called S3 shear zones). Within the test volume, biotite-rich meta-basic dykes appear at both sides of the S3-oriented shear zone. Between the two S3-oriented shear zones the rock mass is highly fractured. From optical televiewer (OPTV) borehole logging and core-logging in in various boreholes, the locations of pre-existing fractures, shear zones, and the orientation of foliation are known. The foliation has an average orientation of 140/80 (i.e. dip direction /dip). Fracture densities and orientations were calculated from the OPTV and core-logging data (Figure 2, 3, and 4). The average fracture density of the undisturbed rock mass, penetrated by the boreholes SBH1 and SBH3, ranges from zero to three fractures per meter (note that no fractures have been observed in SBH1. In contrast, the borehole SBH4 that penetrates an S3 shear zone shows an increasing number of brittle fractures as it approaches the shear zone.

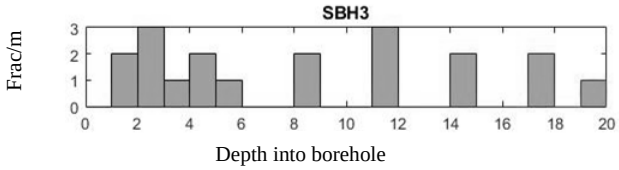

Figure 2 - Fracture densities for SBH-3.

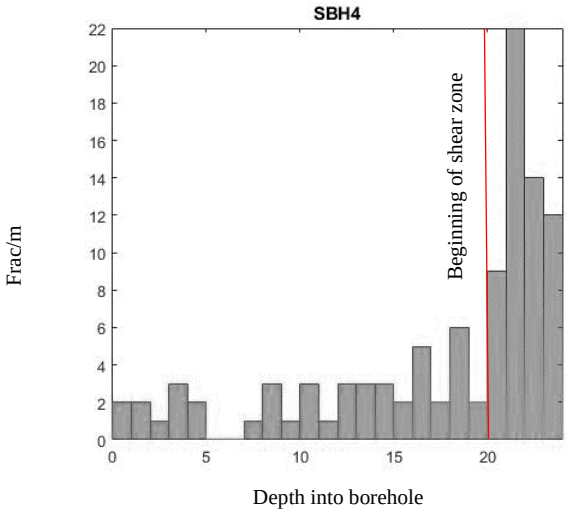

Figure 3 - Fracture density for SBH-4. The vertical line at 20 m marks the beginning of the S3-oriented shear zones

The majority of the structures dip steeply towards southeast, only few fractures dip towards northeast or west (Figure 4).

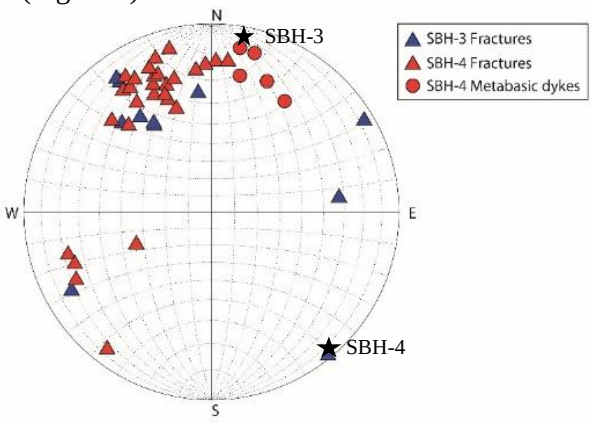

Figure 4 - Lower hemisphere equal-angle stereonet showing orientations of fractures and metabasic dykes from SBH-3 and SBH-4.

3. HYDRAULIC FRACTURING

Hydraulic fractures (HF) were initiated in a 0.7 m interval that was sealed-off by a straddle packer system. The fracture was first initiated during the breakdown cycle and then propagated during multiple reopening cycles. The intervals were chosen using OPTV images to ensure they were free of pre-existing fractures. A total volume ranging from 6.4 l to 14 l was injected per fracture during the breakdown and reopening cycles.

Impression packer surveys were conducted to attempt to define the orientation of the induced fracture traces. Fracture propagation away from the hole was visualized using seismic monitoring. The seismic sensors were located along the tunnel walls, and also inside the SBH-1 borehole for monitoring the tests in SBH-3.

The minimum principal stress, σ_3, was taken as the instantaneous shut-in pressure (ISIP) obtained at the end of the last reopen cycle. The resulting σ_3 estimates in

SBH-1 and -3 vary between 8 and 10 MPa (Figure 5). Those in SBH-4 are consistent with this above 10 m, but progressively decrease along the hole as the S3 shear zone is approached.

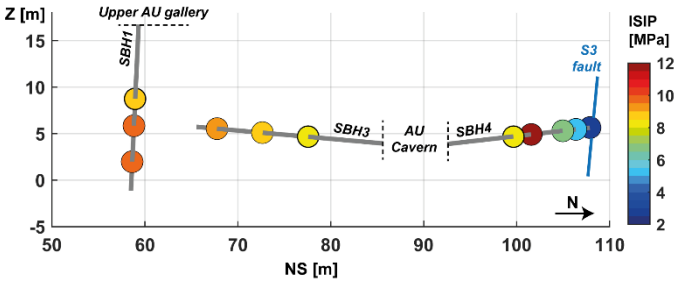

Figure 5- Location of HF experiment with a color-coded indication of ISIP.

Precise location of microseismic events induced by the tests in SBH3, show flattened, high-angle clouds that initiate in the interval and propagate in an EW direction, the average orientation being ~185/75 (dip-direction/dip) (Figure 6). Thus, if σ_3 is normal to the microseismic cloud, it would point towards 005/15. (Gischig et al., 2017) Note that during hydro-fracturing in SBH1 seismic monitoring was not operational, and for SBH4 seismicity is not presented as seismic data are currently being processed.

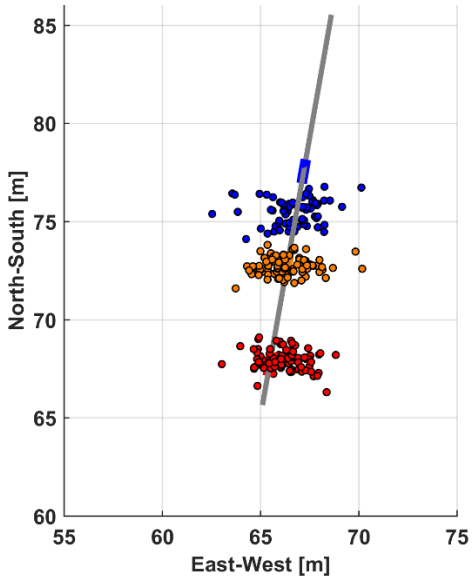

Figure 6- Illustration of the seismic events during the HF experiments in SBH-3. Each color represents one HF-experiment.

The traces of induced fractures along the SBH-1 borehole fit the orientation of the fitted plane through the seismic cloud from SBH-3 with a deviation of ±30° in strike (Figure 7). The HF fracture traces from SBH-3 and the northwest-most HF traces in SBH-1 are almost parallel to the average rock mass foliation (i.e. deviate by 20°).

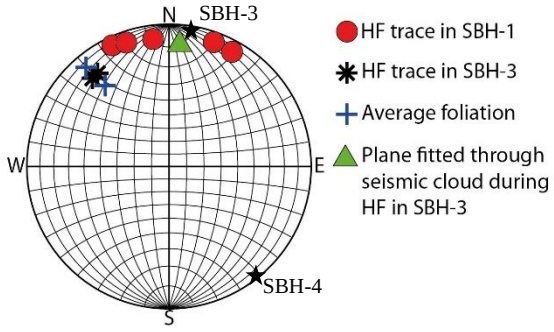

Figure 7 - Combination of the HF orientations measured inside the boreholes (SBH-3 and SBH-4) and inside the rock mass. Additionally, the average orientation of the foliation is plotted

More information concerning the HF-experiments in SBH-4 can be found in Jalali et al. (2017).

4. OVERCORING

4.1. Isotropic analysis

In total 16 overcoring tests were conducted, 10 with a USBM gauge and 6 with a CSIRO Hollow Inclusion (HI) cell (Table 1). Several issues occurred during the tests: 1) a spontaneous increase in water pressure developed during overcoring, 2) difficulties were encountered extracting the overcored specimen without damage, and 3) the curing of the glue for the CSIRO-HI cell was occasionally suspect. Reliable data came only from three CSIRO-HI cell and six USBM overcoring tests. Thus, only the strain datasets from these nine tests were used in the inversions for stress.

Immediately after each overcoring experiment, a biaxial test of the overcore was conducted on site to estimate the elastic parameters of the rock. During each test, the granitic hollow cylinder with the probe inside was subjected to two loading/unloading cycles up to 12 MPa, and the compressive and relaxation strains measured by the gages of the probe were measured. The resulting elastic parameters were used in the inversion of the strains recorded during overcoring to obtain stresses using the equations provided by Amadei and Stephansson, 1997. The initial inversions used an isotropic elastic model. Work towards inverting the data with a transversely isotropic elastic model is on-going, and so the results of inverting only one high-quality CSIRO-HI cell dataset are reported in this paper.

Table 1 - Depths of overcoring measurement probes into boreholes.

	USBM position [m]	CSIRO-HI position [m]
SBH 1	10.4, 11.3, 12.0, 16.0	None
SBH 3	8.3, 14.2, 19.6	9.0, 14.8, 20.0
SBH 4	8.4, 14.2, 18.5	9.2, 14.9, 19.05

The isotropic Young's moduli from on-site biaxial tests range from 20.4 GPa to 25.7 GPa and the Poisson's ratio varies between 0.24 and 0.27 (Bouffier et al., 2015). The isotropic inversion of the CSIRO HI-cell strains using

parameters combinations within these ranges indicates a sub-horizontal major principal stress (σ_1) that points towards SE or NW (i.e. dip-direction 136-144° and 324°) with a magnitude ranging from 20 to 26 MPa (Figure 8).

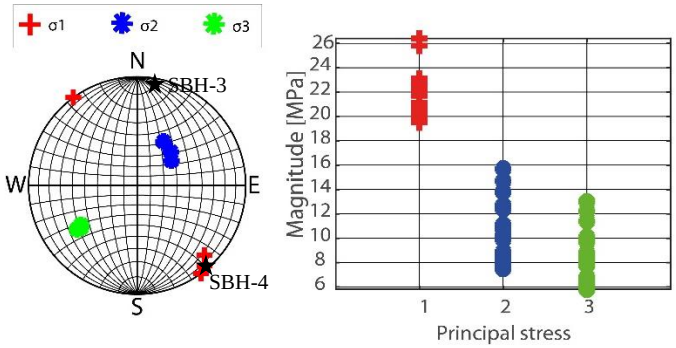

Figure 8- Results of inversions of the three high-quality CSIRO HI-cell tests in SBH-3 and SBH-4 using an isotropic elastic model. left: Orientation of principal stress axes (lower hemisphere equal-angle); right: Magnitudes of the three principal stresses plotted in MPa.

σ_2 and σ_3 were inclined and dip towards NE and SW, respectively. The magnitudes of σ_2 and σ_3 are similar, the maximum difference being 2.7 MPa.

The σ_1 orientation estimates from the isotropic inversion are all consistent and coincide with the direction of the SBH-4 borehole (i.e. 140/05). Accepting this, the USBM probes would directly measure the principal stresses σ_2 and σ_3 in this borehole. The magnitudes are in the range 7.5 MPa to 9.1 MPa for σ_2, and 4.8 MPa to 7.4 MPa for σ_3. These USBM-derived magnitudes tend to be smaller than the CSIRO HI-cell derived ones.

Comparing the results of isotropic overcoring inversion with the results from the HF-experiments reveals a misfit in the principal stress orientations: 1) σ_3 from overcoring is sub-vertical, whereas seismicity during HF suggests a sub-horizontal, NS striking orientation for σ_3; 2) σ_1 from overcoring is not parallel to the microseismic cloud but is inclined by an angle of about 60°. In view of this, we investigated whether the discrepancy can be alleviated using a transverse isotropic inversion of the recorded strain values.

4.2. Transverse isotropic analysis

To invert the measured strain values for the in-situ stress orientations and magnitudes based on a transverse isotropic rock model, all five independent elastic parameters need to be known. This includes the Young's modulus parallel and perpendicular to the plane of isotropy (i.e. E_1 and E_2, respectively), as well as the corresponding Poisson ratios ν_{21} and ν_{31} and the so-called independent cross-shear modulus G_{12}. To constrain these parameters, a transverse isotropic elastic 3D finite element model (COMSOL) was used to simulate the biaxial tests with the CSIRO HI-cell probe inside (Figure 9). The five independent elastic parameters were varied until the CSIRO HI-cell strain measurements predicted by the model fitted the observations. We applied a grid search that was simplified with the following two assumptions:

A) Uniaxial testing of samples in the laboratory revealed an anisotropy, E_2/E_1, of approximately 50% in Young's modulus. Therefore, for most inversions we take,

$$E_1 = 2 * E_2 \,, \tag{1}$$

although in one set of inversions we explore models with lower degrees of anisotropy (Figure 11).

B) The independent shear modulus, G', was approximated using the empirical equation (Saint-Venant, 1863; Worotnicki, 1993):

$$G' = \frac{E_1 * E_2}{E_1 * (1 + 2 * \nu_{12}) + E_2} \tag{2}$$

As a measure of quality-of-fit, we computed the root-mean-squared (RMS) sum of the differences between all 12 modeled and measured strains gauges. Models that produced a lower RMS than obtained from the best isotropic model are assumed to be more realistic than the isotropic inversion.

Thus, sets of transversely isotropic elastic parameters that yielded a lower RMS value when applied to the biaxial test data than the RMS from the isotropic model were identified. These were then used to invert the strains recorded during overcoring to obtain stress tensor solutions.

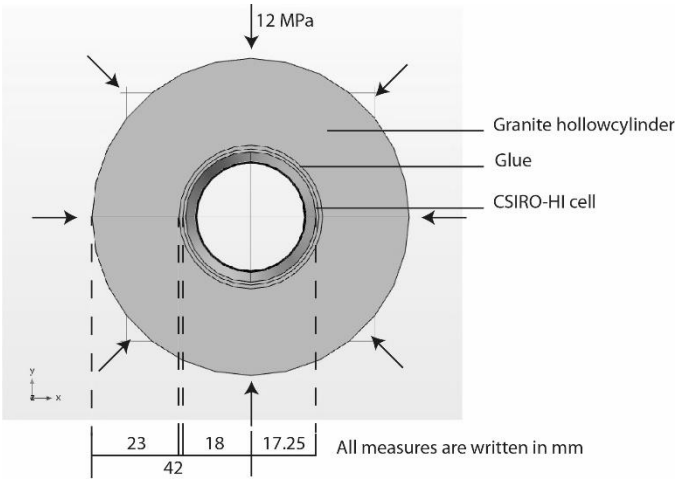

Figure 9 – Cross-section through the recovered overcore showing the loading in the biaxial test and the CSIRO HI cell bonded inside the hollow granite cylinder.

Here we present the results of the anisotropic inversion of the CSIRO HI-cell strain data recorded during the test conducted in SBH-3 at 9.0 m depth (denoted as Test SBH-3-2). Table 2 lists the elastic parameter values, defined on the basis of the biaxial test, that were used in combination in the inversions. For most inversions, eqn. 1 was applied (i.e. $E_1 = 2E_2$) and hence the number of free parameters

was 3. Combinations of the free parameter values were randomly chosen for the inversions. For the case when $E_1 = 2E_2$, a total of 1280 models where generated. Note that although the ranges of the parameters in Table 2 were chosen on the basis that when used in some combination with the others in modeling the biaxial test data, they produced RMS values that were lower than obtained using the isotropic model, this was not necessarily the case for all random combinations of the parameters.

Table 2 – Parametric grid for transverse isotropic inversion;

E_1 [GPa]	17, 19, 21, 23, 25
ν_{21}	0.15, 0.16, 0.17,…..,0.3 (16 values in all)
ν_{31}	0.15, 0.16, 0.17,…..,0.3

Before identifying the combinations of parameters in Table 2 that yielded the best-fit to the biaxial test data (i.e. lowest RMS), we first examined the effect of varying Young's modulus and Poisson's ratio on the stress solutions obtained by inverting the overcoring strain data. For this study, eqns 1 and 2 were respected, and combinations of the three independent parameters, E_1, ν_{21}, and ν_{31} varied over the ranges given in Table 2**.** The resulting range of stress solutions obtained is shown in Figure 10. Evidently, all principal stress magnitudes are lower than obtained using the isotropic rock model, the reduction being greater for smaller values of Young's modulus, E_1 (and by implication, E_2). The σ_1 magnitude ranges between 11 MPa and 19 MPa, with the higher values corresponding to greater E_1 values. The σ_2 and σ_3 magnitudes range from 7 MPa to 17 MPa and 7 MPa to 13 MPa, respectively. Clearly, anisotropy has a strong effect on the principal stress magnitudes. The effect of varying Poisson's ratio has a lesser effect on magnitude than Young's modulus (see caption of Figure 10).

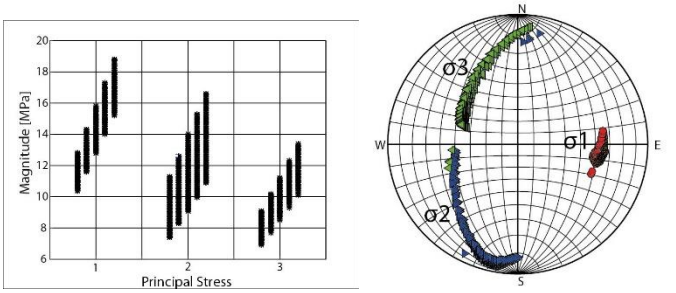

Figure 10 –Principal stress solutions obtained by inverting the strains for the test at 9 m depth in SBH-3 using the transverse isotropic rock models. Left: Principal stress magnitudes. The effect of varying Young's modulus from 17 GPa to 25 GPa is shown by the five offset grey lines for each principal stress, and the length of the lines denotes the effect of varying the Poisson's ratios. Right: Corresponding principal stress orientations (lower hemisphere, equal area projection).

The principal stress orientations are also strongly affected by the anisotropy. The orientation of σ_1 dips towards the east at almost 35°, and is remarkably insensitive to the parameter values. In contrast, the orientation of σ_2 and σ_3 varies greatly with the elastic parameters, which is a consequence of the near-equality of their magnitudes.

A further series of inversions was performed to study the effect of the strength of the anisotropy. For these, the ratio E_2/E_1 was varied from 0.5 to 1.0, whilst allowing E_1 to vary between 17-25 GPa, ν_{13} to vary between 0.2 and 0.3, and keeping ν_{12} constant at 0.25.

The stress orientation solutions obtained from the inversion are shown in Figure 11. For a given anisotropy ratio, the principal stress orientations form distinct clusters with very little variation throughout the range of variation of the elastic parameters. However, changing the ratio has a significant effect on the orientations. Thus, the orientation of the principal axes is predominantly affected by the strength of the anisotropy as defined by the ratio E_2/E_1. Varying the degree of anisotropy in steps of 12.5 percent from 1.0 to 0.5 serves to rotate σ_1 by almost 50° (Figure 11).

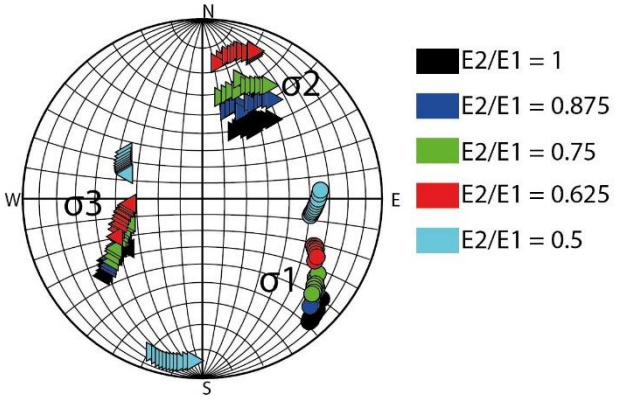

Figure 11 – Principal stress orientation solutions obtained from models that have distinct ratios of E_2/E_1.

We now return to the identification of the combinations of parameters in Table 2 that yield the best fits to the biaxial test data. This was done by calculating the RMS values obtained for each parameter combination. Eqn 1 was taken as valid (i.e. $E_1 = 2E_2$) and hence there were 3 free parameters. During the SBH-3-2 overcoring test, only 8 out of 12 gauges yielded consistent strains, the other four showing unrealistically low strains, possible due to glue creep. Thus, the RMS value was obtained by summing the individual RMS values for the 8 functioning gauges. Only the strains recorded during the second of two loading cycle were considered.

The summed RMS values obtained by systematically varying the parameters over the ranges given in Table 2 (noting that $E_1 = 2E_2$) are shown in Figure 12. The values range from ~205 to ~450 μ-strain, the minimum being obtained for $E_1 = 21$ GPa. The best-fitting isotropic model using the parameters obtained by INERIS (Bouffier et al., 2015) had an RMS of ~231 μ-strain. As noted earlier, models that use combinations of transversely isotropic elastic parameters which yield an RMS value less than this are considered to be more realistic than the isotropic

model, and thus were used for the final inversion. Figure 12 indicates this criterion is met for models with E_1 of 19 GPa, 21 GPa and 23 GPa, lower values of ν_{13} and all values of ν_{13}.

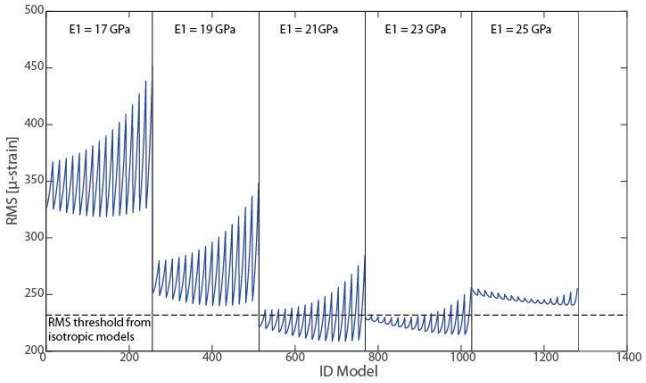

Figure 12 Calculated RMS values for the transverse isotropic models for which $E_1 = 2E_2$. The value of E_1 increases in blocks from left to right. The 'saw-tooth' variations in RMS corresponds to the systematic variation of the Poisson ratios, ν_{12} and ν_{13} over the ranges in Table 2. Within each block of given E_1, the initial rise reflects the effect of increasing ν_{13} between 0.15 and 0.3 whilst ν_{12} is constant at the initial value of 0.15. Then ν_{12} is reset to 0.16 and ν_{13} again varied from 0.15 to 0.3, producing the second rise, and so on. The dashed horizontal line denotes the RMS threshold from the isotropic model.

Figure 13 shows stress solutions obtained by inverting the overcoring strains using transverse isotropic elastic parameter sets that, when used to invert the biaxial test data, yielded RMS values that are less than the threshold values derived from the isotropic model. The σ_1 estimates range between 13 and 17 MPa, σ_2 ranges from 9 MPa to 14 MPa, and σ_3 from 8.7 MPa to 11.9 MPa. The HF results indicate $\sigma_3 < 10$ MPa. Imposing this additional constraint restricts the solutions to the subset at the lowermost range of magnitudes (green in Figure 13). The orientation of the σ_1 principal axis is remarkably well defined as dipping 35-40° towards east, and shows little variation with parameter set, regardless of whether the $\sigma_3 < 10$ MPa constraint is applied. In contrast, the orientation of the σ_2 and σ_3 axes is not well defined because of the near-equality of their respective magnitudes.

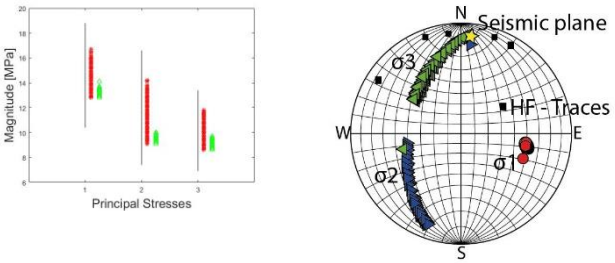

Figure 13- Stress solutions obtained by inverting the overcoring strains using elastic parameter sets that yield RMS values from the biaxial test inversions that are less than the threshold derived from the isotropic model. Upper Part: magnitudes of the three principal stresses, the green circles are the subset of solutions that satisfy the additional constraint that $\sigma_3 \leq 10$ MPa. Lower Part: Principal stress orientations, which are relatively stable and independent of the magnitudes. Stereo plot a) shows all stress solutions with an RMS value below the isotropic one, and stereo plot b) visualizes all stress solutions from a) that have a $\sigma_3 \leq 10$ MPa.

5. DISCUSSION

The conventional interpretation of hydrofracture tests holds that the fracture develops in a plane normal to the minimum principal stress. In situations where the borehole axis is not normal to the minimum principal stress, the tendency of the hydrofracture test interval to fracture axially during pressurization can result in complex fracture initiation in the near-well region, and fracture reorientation to the plane normal to the minimum principal stress during propagation. This reorientation can occur rapidly outside the wellbore stress concentration (Warren and Smith, 1985). The pattern of microseismicity recorded during each of the hydrofracture tests in SBH-3 consistently show a quasi-planar structure that strikes E-W and dips at 80° to the south (Figures 6 and 7). Taken on face value, this would suggest a sub-horizontal σ_3 oriented N-S with a magnitude of 8-10 MPa. This is consistent with the observed axial traces of the fractures induced during the hydrofracture tests in the sub-vertical SBH-1 borehole (unfortunately, the microseismic system was not fully-functional during these tests). It might also explain the complex nature of the two traces of the induced fractures in the SBH-3 hydrofracture tests (Figure 7).

The overcoring tests interpreted with an isotropic elastic model do not yield stress solutions that are consistent with a sub-horizontal, N-S directed orientation for σ_3. Specifically, they suggest a stress state where σ_1 is sub-horizontal and oriented N140-150°E, with a magnitude of 19-26 MPa. However, consideration of transverse anisotropy in the model used to invert the overcoring strains appears to bring the stress solution into consistency with the hydrofracture and microseismicity observation, at least for the single high-quality overcoring test we have so far analyzed in this way. Uniaxial tests on core samples show that the elastic anisotropy is large, the Young's modulus for loading normal to the foliation plane, E_2, being only half that for in-plane loading, E_1. Parameter studies showed that the magnitudes of the principal stresses are more strongly influenced by the absolute value of the Young's moduli than by their relative ratio, E_2/E_1. However, the opposite is true for the orientations of the principal axes.

Taking E_2/E_1 as 0.5, a range of best-fitting elastic models were defined from combinations of transverse isotropic elastic parameters that best reproduced (in an RMS residual sense) the strains recorded during the biaxial tests of the overcore sample. Inversion of the overcoring strains using these models yielded stress solutions with σ_1 of magnitude 13-17 MPa and plunging 30-40° to east, thereby lying within the plane of the microseismicity and normal to the axis of the borehole SBH-3. The magnitudes

of σ_2 and σ_3 from the solutions were comparable, the σ_3 estimates being 8.7 - 11.9 MPa, which is consistent with the hydrofracture-derived σ_3 estimates of 8-10 MPa. Limiting the overcore-derived solutions to consistency with $\sigma_3 < 10$ MPa yields relatively tight constraints on the magnitude of all principal stresses, the range of magnitudes of σ_2 being almost identical to σ_3. Thus, the orientation of σ_2 and σ_3 were not well-defined, other than lying in the plane normal to σ_1.

The best-fit stress solution from the overcore tests at SBH-3-2 inverted using the transverse isotropic model is consistent with the hydrofracture and microseismicity observations inasmuch as it indicates that σ_1 lies in the plane of the microseismic structure, and the stress acting normal to the plane would be essentially σ_3. Given the near-equivalence of σ_2 and σ_3, it is perhaps surprising that the orientation of the microseismic planes is so consistent. A further question is why the trace of one of the two sub-axial induced hydrofractures in borehole SBH-3 was sub-vertical, when a sub-horizontal would be favoured from the best-fit stress solution. Future work will address these issues, and extend the transverse-isotropic analysis to include the other high-quality overcoring tests.

6. CONCLUSION

The application of several different techniques proved crucial for the satisfactorily characterization of the state of stress within the experimental rock mass at the Grimsel Test Site. Hydrofracture stress measurements with concomitant monitoring of the attendant induced microseismic activity yielded largely consistent results which suggested that the minimum principal stress was sub-horizontal and oriented north-south. The minimum principal stress magnitude was 8-10 MPa. Overcoring tests were conducted using both USBM and CSIRO HI-cell probes with the primary objective of determining the magnitude and orientation of the principal stresses. Inversion of the overcoring strains using an isotropic elastic model with moduli derived from on-site biaxial testing of the overcore sample yielded a very high value for σ_1 and an orientation for σ_3 that was not in accord with the hydrofracture- and microseismicity-derived results. However, the discrepancy in σ_3-orientation largely disappeared when a transverse isotropic model was used with a ratio of normal-to-foliation and in-plane Young's moduli of 0.5, as measured in uniaxial tests on core samples. To date, only overcore data from one high-quality CSIRO HI-cell has been inverted with the transverse isotropic model. The results indicate that σ_1 has a magnitude 13-17 MPa and a plunge of 30-40° to the east, thereby lying within the plane of the microseismicity. The magnitudes of σ_2 and σ_3 from the solutions are comparable, the σ_3 estimates being 8.7 - 11.9 MPa, which is consistent with the hydrofracture-derived σ_3 estimates of 8-10 MPa.

ACKNOWLEDGEMENT

Funding for this project was provided by the Swiss commission for technology and innovation (CTI), EKZ Zürich and Shell through the Swiss Competence Center for Energy Research – Supply of Electricity (SCCER-SoE). Additionally, this project was funded by the SNF-project 2-77205-16.

REFERENCES

1. Amadei, B., and O. Stephansson. 1997. Rock stress and its measurement. *Springer Science & Business Media*.
2. Amann F., J. Doetsch, V. Gischig, M.R. Jalali, K.F. Evans, B. Valley, C. Madonna, M. Klepikova, H. Krietsch, A. Kittilä, D. Giardini, S. Wiemer, M. Saar, H. Maurer, Simon Löw and T. Driesner. 2017. An in-situ stimulation experiment at the Grimsel Test Site (*in-preparation*).
3. Bouffier, C., F. Lahaie, and P. Bigarre. 2015. Stress measurements by overcoring at the Grimsel site – Results from the campaign of August-September 2015., *INERIS, Technical Report*
4. Evans, K.F., and T. Engelder. 1989, Some problems in estimating stress magnitudes in thrust stress regimes. *Int. J. Rock Mech. Min. Sci. & Geomech. Abstr., 26(6)*, 647-660
5. Gischig, V.S., J. Doetsch, H. Maurer, H. Krietsch, F. Amann, K.F. Evans, M. Nejati, M.R. Jalali, A. Obermann, B. Valley, S. Wiemer, and D. Giardini. 2017. On the link between stress field and small-scale hydraulic fracture growth in anisotropic rock derived from mirco-seismicity. (*In preparation)*
6. Jalali, M.R., V. Gischig, J. Doetsch, H. Krietsch, F. Amann. 2017. Mechanical, Hydraulic and Seismological Behavior of Crystalline Rock as a Response to Hydraulic Fracturing at the Grimsel Test Site. In *Proceedings of 51st US Rock Mechanics / Geomechanics Symposium*. San Francisco, CA, USA.
7. Konietzky, D. H. 1995. 3d stress filed and 2d disturbed zone modelling for the Grimsel Test Site. *Technical report, NAGRA.*
8. Pahl, A., S. Heusermann, V., V. Braeuer, and W. Gloeggler. 1989. Rock stress investigations. *Technical report, NAGRA.*
9. Saint-Venant, B. 1863. Sur la distribution des élasticités autour de chaque point d'un solide ou d'un milieu de contexture quelconque. *J. de Mathématiques Pures et Appliquées.* 7-8, 353-430, 257-261. (in French).
10. Warren, W.E., and C.W. Smith. 1985. In situ stress estimates from hydraulic fracturing and direct observation of crack orientation. *J. Geophys. Res., 90*, 6829-6839
11. Worotnicki G. 1993. CSIRO triaxial stress measurement cell. *Comprehensive Rock Engineering* (Edited by

Hudson, J.A.), Chap. 13, Vol. 3, pp. 329-394. Pergamon, Oxford.